ORIGINAL RESEARCH ARTICLE

Imaging properties of radiative multi-sub mirror array structure

Xiaoyao Liu[1*], Zhongcheng Liang[1], Weiqian Hao[1], Rui Zhao[1], Meimei Kong[1], Tao Chen[1], Yue Zhang[2]

[1] School of Electronic and Optical Engineering, School of Microelectronics, Nanjing University of Posts and Telecommunications, Nanjing 210023, China. E-mail: 1761590525@qq.com*

[2] Beijing Institute of Space Mechatronics, China Academy of Space Technology, Beijing 100094, China.

ABSTRACT

Based on the characteristics of liquid lens sparse aperture imaging, a radiative multiplet array structure is proposed; a simplified model of sparse aperture imaging is given, and the analytical expression of the modulation transfer function is derived from the optical pupil function of the multiplet array structure; the specific distribution form of this multiplet array structure is given, and the structure parameters are approximated by the dimensionless method; the two types of radiative multiplet array structures are discussed, and the filling factor, redundancy, modulation transfer function and other characteristic parameters are calculated. The physical phenomena exhibited by the parametric scan are discussed, and the structural features and imaging characteristics of these two arrays are compared. The results show that the type-II structure with larger actual equivalent aperture and actual cutoff frequency and lower redundancy is selected when the average modulation transfer function and the IF characteristics of the modulation transfer function of the two structures are close to each other; the type-II structure has certain advantages in imaging; the conclusion is suitable for arbitrary enclosing circle size because the liquid lens-based multiplet array structure adopts dimensionless approximation parameters; compared with the composite toroidal structure, the radiative multiplet mirror structure has a larger actual cut-off frequency and actual equivalent aperture when the filling factor is the same.

Keywords: Imaging System; Modulation Transfer Function; Liquid Lens Array; Sparse Aperture; Optical Pupil Function

1. Introduction

High-resolution imaging is widely used in feature detection, urban mapping, agricultural and forest monitoring, small target detection, etc., and plays an extremely important supporting role in national economic development and national defense construction. In the diffraction limit, the angular resolution of an optical system is the ratio of the working wavelength to the pupil aperture, which indicates that only large-aperture optical systems can have high spatial resolution. However, it is difficult and costly to manufacture and inspect large-aperture mirrors[1], and large-aperture mirrors will lead to larger size and mass of the telescope, which makes the development of the telescope extremely difficult. Sparse aperture[2] imaging system is one of the effective solutions to solve the above difficulties. The so-called sparse aperture is to form a certain form of array structure of multiple small-aperture sub-mirrors to form a large optical aperture to overcome the trouble caused by the large aperture of the optical system. According to Liu *et al.*[3], Yi *et al.*[4], Wu *et al.*[5], Wu *et al.*[6], Harvey and Rockwell[7], the array structure of sparse aperture has Golay structure, ring structure, three-arm structure, compound three-sub-mirror structure, and multi-

circular structure. As the number of apertures increases above 20, the maximum filling factor of these sparse aperture structures decreases to about 15%[8]. Fiete *et al.*[9] showed that the filling factor of the system should be increased as much as possible while considering the cost and volume.

Based on the research of liquid lens[10,11], our group proposed a liquid lens sparse aperture array structure. Since the size of the liquid lens cannot be too large due to the fabrication limitation, and the design of the sparse aperture array structure requires a high filling factor, the number of sub-mirrors of this sparse aperture array should be large. Of course, the increase in the number of sub-mirrors will bring a series of technical problems for future experiments, such as the preparation of liquid lens, array mechanism, phase detection, and IF compensation[12], so the array needs to be optimally designed. In this paper, we propose a radiation-like multiplexed mirror array structure and theoretically analyze the structural characteristics and imaging performance of this multiplexed mirror array.

2 Basic theory of optical sparse aperture imaging

2.1 Simplified model of imaging system

The simplified model of the optical sparse aperture imaging system[13] is shown in **Figure 1**. Where: the quasi-monochromatic plane light source is located on the front focal plane x_0y_0 $x_0y_0$of lens L_1, which is used to simulate the light intensity distribution of distant objects; the observation area is located on the back focal plane $x_{i'}y_{i'}$ $x_i'y_i'$of lens L_2 (i' is the location of the observation point), which is used to simulate the light intensity distribution on the image plane; f_1 and f_2 are the front focal distance of lens L_1 and the back focal distance of lens L_2, respectively; The clear aperture of any shape on the plane xy is the area P, which is used to simulate the light pupil function of the imaging system.

The light intensity distribution of the distant object plane is assumed to be $I_0(x_0,y_0)I_0(x_0,y_0)x_0y_0$. In the case of quasi-monochromatic noncoherent illumination, the light intensity distribution on the image plane of the optical sparse aperture imaging system is:
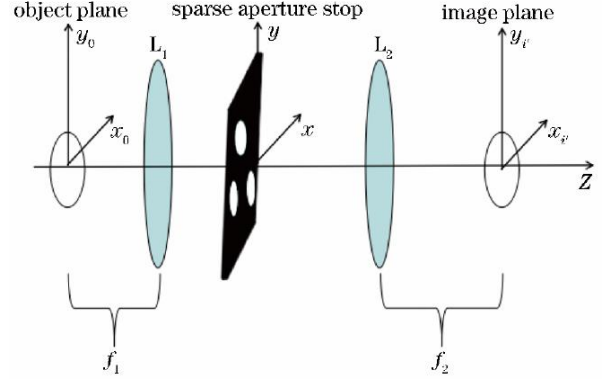
Figure 1. Simplified model of optical sparse aperture.

$$I_{i'}(x_{i'},y_{i'}) = I_g(x_{i'},y_{i'}) * g_{PSF}(x_{i'},y_{i'})$$
(1)

where: I_g is the geometric ideal image of the imaging target; g_{PSF} is the point spread function (PSF) of the system. The equation (1) indicates that the image formed by the system is equal to the convolution of the geometric ideal image of the imaging target and the point spread function of the system.

In the frequency domain, we have
$$I_{i'}(f_x,f_y) = I_g(f_x,f_y) * g_{OTF}(f_x,f_y)$$
(2)

where: f_x and f_y are the spatial frequencies along the x and y directions respectively; g_{OTF} is the optical transfer function (OTF) of the system. The equation (2) indicates that the spectrum of the system imaging is equal to the product of the spectrum of the ideal image of the imaging target and the optical transfer function of the system. The g_{OTF} of the system is non-zero only in a finite range and decreases monotonically to zero after a certain frequency.

2.2 Optical pupil function

According to Fourier optics theory[13], the optical modulation transfer function is used to describe the imaging performance of an optical system in the frequency domain. The optical modulation transfer function (MTF) is the ratio of the spectrum of the actual image of the imaging system to the spectrum of the ideal image of the target, reflecting the ability of the imaging system to transfer the frequency components contained in

the target light intensity distribution to the image plane. Pupil function only has 2 values of 1 or 0. Optical modulation transfer function is the autocorrelation operation and modulo of pupil function.

The specific calculation method is as follows: for a radial multi-mirror imaging system composed of N circular apertures with diameter d and radius a, taking the three clusters of radial multi-mirror structures corresponding to $z = 2$ in **Figure 2** as an example, the pupil function $p\,(x,y)$ can be mathematically expressed as the convolution of a sub-aperture pupil function and a delta function array, namely:

$$\mathrm{p(x,y)} = \mathrm{circ}\left(\frac{\sqrt{x^2+y^2}}{\frac{d}{2}}\right) * \sum_{i,j,k} \delta(x - r_{kj}\cos\theta_{ki} \cdot y - r_{kj}\sin\theta_{ki}) \cdot k, \; k = 1,2,3$$

(3)

where: circ (•) is the circle function; * is the convolution; r_{kj} is the distance from the center of the enclosing circle to the center of each subaperture; θ_{kj} is the orientation of each branch; i is the number of branches; j is the number of subapertures on each branch. When, $k = 1, 2, 3$, respectively, we have

$$\begin{cases} r_{kj} = j\Delta r, j = 1,2,\dots,n_1 \\ \theta_{ki} = \frac{2\pi}{3}(i-1) + \frac{\pi}{6}, i = 1,2,3 \end{cases}$$

(4)

$$\begin{cases} r_{kj} = (n_1 - n_2)\Delta r + j\Delta r, j = 1,2,\dots,n_2 \\ \theta_{ki} = \frac{2\pi}{3}(i-1) + \frac{\pi}{2}, i = 1,2,3 \end{cases}$$

(5)

$$\begin{cases} r_{kj} = (n_1 - n_3)\Delta r + j\Delta r, j = 1,2,\dots,n_3 \\ \theta_{ki} = \frac{\pi}{3}(i-1) + \frac{\pi}{2}, i = 1,2,\dots,6 \end{cases}$$

(6)

where: Δr is the spacing between sub-mirrors; n_1, n_2 and n_3 are the number of sub-mirrors on each branch of cluster 0, cluster 1 and cluster 2, respectively.

2.3 Modulation transfer function expressions

The modulation transfer function α_{MTF} α_{MTF} is obtained by Fourier transforming equation (3) and taking the modulus as

$$\alpha_{\mathrm{MTF}} = \alpha_{\mathrm{MTF},d} + \frac{1}{N}\alpha_{\mathrm{MTF},d} *$$

$$\sum_{m=1}^{N-1}\sum_{n=m+1}^{N} \delta\left(f_x \pm \frac{x_n - x_m}{\lambda f}, f_y \pm \frac{y_n - y_m}{\lambda f}\right)$$

(7)

where: $\alpha_{\mathrm{MTF},d}$ is the modulation transfer function for a single subaperture; m and n are the summation indices for the subapertures; λ is the wavelength; f is the distance from the optical pupil to the image plane; $N = 3n_1 + 3n_2 + 6n_3$; $\delta(\cdot)$ is the Dirac function; coordinates (x_m, y_m) and (x_n, y_n) contain all of the radial multiplet circle center coordinates.

The modulation transfer functions $\alpha_{\mathrm{MTF},d}$ for a single subpath are

$$\alpha_{\mathrm{MTF},d} = \begin{cases} \frac{2}{\pi}\left\{\arccos\frac{\rho}{\rho_d} - \frac{\rho}{\rho_d}\left[1 - \left(\frac{\rho}{\rho_d}\right)^2\right]^{\frac{1}{2}}\right\}, & 0 \leqslant \rho \leqslant \rho_d \\ 0, & \rho > \rho_d \end{cases}$$

(8)

where: ρ_d is the cutoff frequency of the subaperture whose diameter is d, $\rho_d = d/(\lambda f)$; ρ is the spatial frequency.

From the above calculation, it can be seen that the modulation transfer function of multiple sub-mirrors is combined by the modulation transfer function of sub-mirrors. By adjusting the relative positions $(x_n - x_m, y_m - y_n)$ between the sub-mirrors to meet the requirements of the modulation transfer function, the optimization can be achieved.

3. Radial multi-mirror array structure

The radial multi-mirror array structure consists of several sub-mirrors of diameter d, which can be divided into clusters of z ($z = 0, 1, 2, \dots$). Cluster 0 has 3 branches, each with n_1 sub-mirrors and orientation of $\emptyset_i = 2\pi(i-1)/3 + \pi/6$, $i = 1, 2, 3$. Cluster 1 has 3 branches; the number of sub-mirrors on each branch is n_2, and the orientation of each branch is $\emptyset_i = 2\pi(i-1)/3 + \pi/2$, $i = 1, 2, 3$. Cluster 2 has 6 branches, the number of sub-mirrors on each branch is n_3, and the orientation of each branch is $\emptyset_i = \pi(i-1)/3$, $i = 1, 2, \dots, 6$. The z cluster has $3 \cdot 2^{z-1}(z \geq 3)$ branches with n_{z+1} sub-mirrors on each branch and orientation of each branch $\emptyset_i = \pi(3 \cdot 2^{z-1}) + \pi(i-1)/(3 \cdot 2^{z-2})$, $i = 1, 2, \dots, 3 \cdot 2^{z-1}$.

Figure 2 corresponds to the three-cluster radial

multiplet structure at $z = 2$. In this paper, we discuss and analyze the multiplet mirror structure in this case as an example.
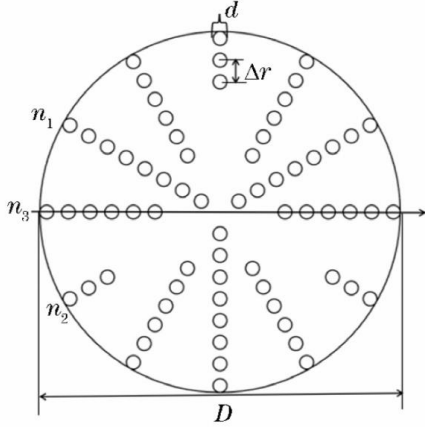
Figure 2. Schematic of radial multi-sub-mirror array structure.

For the radiative multiplet structure, there are five independent parameters d, n_1, n_2, n_3, and Δr when $z = 2$. In order to give the universal law of this multiplet mirror structure, the basic structure parameters are normalized in Δr, i.e., $d_0 = d/\Delta r$, $D = (2n_1 + d_0)\Delta r$, and the normalized structure has 4 independent parameters, d_0, n_1, n_2, n_3. The values of the dimensionless subaperture-approximated diameters d_0 are in the range $0 < d_0 \leq 1$. From the analysis, it can be seen that the number of sub-mirrors in each direction of the radial multi-mirror structure is limited as follows: $n_1 \geq n_2$, $n_1 > n_3$, $n_2 \neq n_3$. In the case that n_1 is determined, the number of sub-mirrors n_2 and n_3 in cluster 1 and cluster 2 of the radial multiplet is different, so the structure can be divided into two different forms: $n_2 > n_3$ for type I and $n_2 < n_3$ for type II. **Table 1** shows the parameters of type I and type II radial multiplet structures when $n_1 = 3$, where $F_{\max}$ is the maximum filling factor.

When n_1 is fixed, there are $(n_1 - 1)(n_1 - 1)$ array structures. Taking $n_1 = 3$ as an example, in order to investigate the imaging characteristics of the type I and type II structures, the radiative multiplet mirror structures with the same number of sub-diameters are selected for comparison, i.e., $n_1 = 3$, $n_2 = 3$, $n_3 = 1$ (type I-331) and $n_3 = 3$, $n_2 = 1$, $n_3 = 2$ (type II-312).

Table 1. Parameters of type I and type II radial multi-sub-mirror structures when $n_1 = 3$

Type	n_2	n_3	N	$F_{\max}$/%
	2	1	21	43
Type I	3	1	24	49
	3	2	30	61
Type II	1	2	24	49

4. Properties of radial multiplet mirrors

4.1 Filling factor

The filling factor F is the ratio of the sparse aperture flux area (the sum of the sub-mirror flux areas) to the enclosed aperture area. For the radial multiplet structure, the filling factor F is

$$F = \frac{Nd^2}{D^2} = \frac{3n_1 + 3n_2 + 6n_3}{(2n_1/d_0 + 1)^2}$$

(9)

Figure 3 shows the relationship between the filling factor F and the dimensionless subaperture-approximated diameter d_0 when $n_1 = 3$. It can be seen that when the total number of subapertures N is fixed, as d_0 increases, the denominator of equation (9) decreases, and therefore the filling factor increases. The maximum filling factor $F_{\max}$ is obtained at $d_0 = 1$:

$$F_{\max} = \frac{3n_1 + 3n_2 + 6n_3}{(2n_1 + 1)^2}$$

(10)
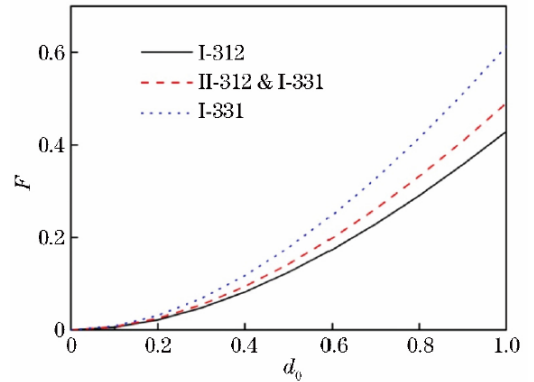
Figure 3. Fill factor F as a function of dimensionless subaperture simplification diameter d_0 in different structures.

At this point, each multinomial mirror is tangent to each other. From the equation (9), it can be concluded that the contribution of n_3 is larger than that of n_2 to make the fill factor increase.

4.2 Redundancy

In the case of the same diameter, the lower the
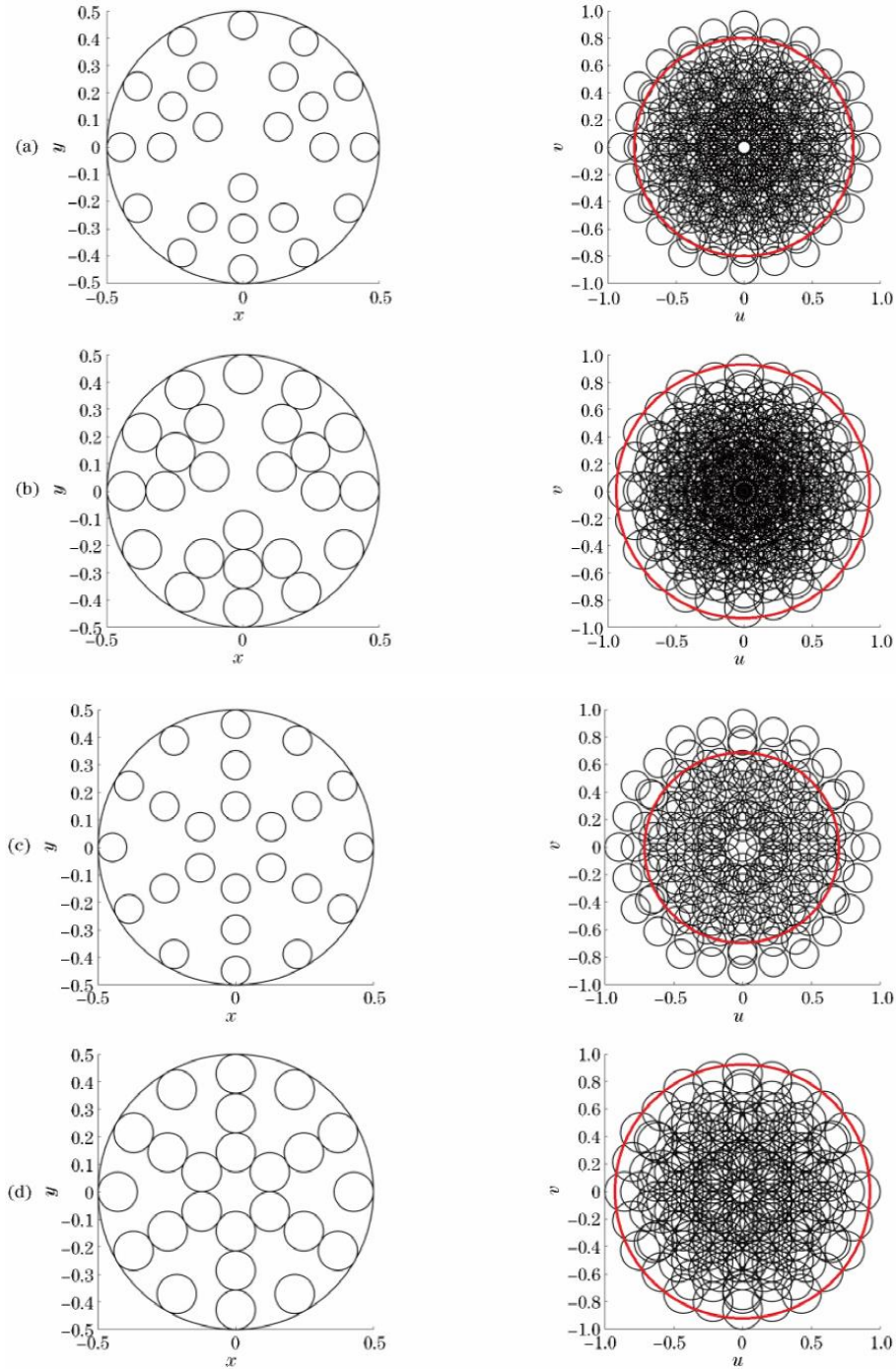
Figure 4. Optical pupil diagrams and MTF profiles of two different structures with different fill factors. **(a)**: type II312 structure when $F = 26\%$; **(b)**: type II-312 structure when $F = 26\%$; **(c)**z: type I-331 structure when $F = 26\%$; **(d)**: type I-331 structure when $F = 49\%$.

redundancy is, the better. The redundancy is defined as the ratio of the number of overlapping submodulation transfer functions in the frequency domain (except for the number of overlapping frequency centers) to $N(N\text{-}1)$. The redundancy is quantitatively calculated to be 1.33% for the II-312 structure and 7.33% for the I-331 structure. The pupil diagrams and modulation transfer function contour diagrams of the two different structures are shown in **Figure 4**, where x and y are the pupil coordinates

and u and v are the spectral coordinates. Comparing **Figure 4a** and **4c** with **Figure 4b** and **4d**, it can be seen that the symmetry of the sub-modulation transfer function of the I-331 structure is significantly higher than that of the I-312 structure, indicating that the redundancy of the I-331 structure is higher, which is consistent with the results obtained from quantitative calculations. The redundancy degree is reduced because the first circumference of type II-312 structure from inside-out is a non-re-

dundant Golay3-type structure, and the second circumference of type II-312 from inside-out is a non-redundant nine-aperture structure with a non-uniform circumference. The I-331 type structure is a uniform circumferential redundant structure with six apertures in the 1st circumference from inward to outward, and there are more than one pair of subapertures in a specific direction in the frequency domain, and repeated sampling for a specific spatial frequency will lead to a higher redundancy of the I-331 type structure. Under the same filling factor, the increase of aperture array redundancy can weaken the response of modulation transfer function to some spatial frequency directions, and the probability of modulation transfer function value of 0 increases, resulting in higher actual cutoff frequency of II-312 type structure than I-331 type structure. In order to reduce the redundancy, the type-II structure with $n_2 < n_3$ can be chosen in the case that the number of sub-mirrors n_1 on each branch of cluster 0 is determined.

4.3 Modulation transfer function

Figure 5 shows the top view of the modulation transfer function for the II-312 and I-331 arrays with fill factors of 14%, 26% and 49%, which shows that as the fill factor increases, the actual cutoff frequency of the system increases and the "holes" in the modulation transfer function become smaller and smaller. The multiplet mirrors are symmetrically distributed in the plane of the pupil entrance, so that the arrangement of $\alpha_{\mathrm{MTF},d}$ in different directions in the frequency domain will also be symmetrically distributed by equation (3). The multi-directional arrangement of the multimirror array structure leads to the maximum and minimum cutoff frequencies tend to be uniform and show a certain pattern. When the fill factor is 14%, a region with a modulation transfer function value of 0 appears between the central main valve and the side valve. When the fill factor is 26% and 49%, the modulation transfer function of II-312 structure is evenly distributed, while the number of baselines of different lengths of I-331 structure is larger in the low frequency range, which leads to too much frequency information passing through the low frequency region and the modulation transfer function is concentrated at the low frequency. The II-312 structure has a larger frequency coverage area and a higher actual cutoff frequency, and the mid-frequency is also flatter.

Figure 6 shows the cross sections of the normalized modulation transfer function in the horizontal and vertical directions for the II-312 and I-331 array structures, where f_{MTF} is the modulation transfer function at the cutoff frequency. **Figures 6a** and **6c** show the cutoff frequencies of II-312 and I-331 structures in the horizontal direction, which shows that: when the filling factor is 14%, the
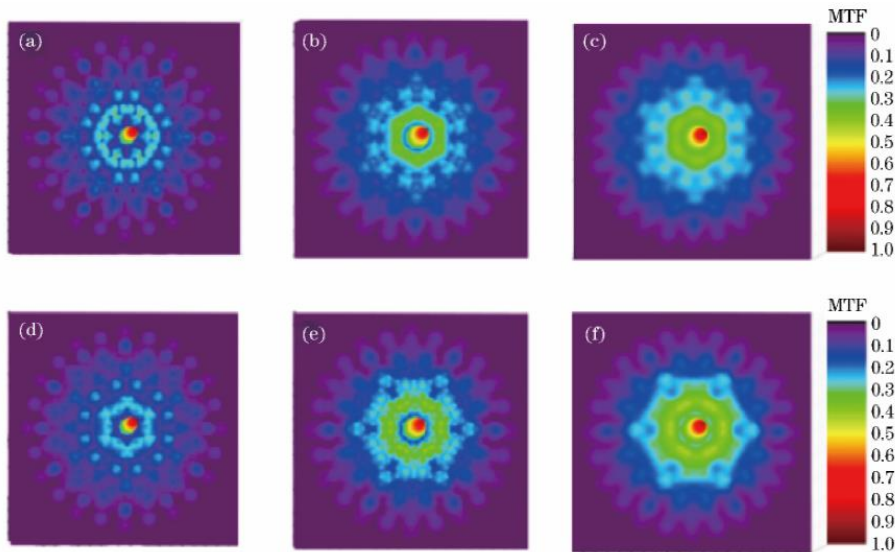
Figure 5. Top views of MTF of two array structures with different fill factors. (**a**): type II-312 structure when $F = 14\%$; (**b**): type II-312 structure when $F = 26\%$; (**c**) type II-312 structure when $F = 49\%$; (**d**) type I-331 structure when $F = 14\%$; (**e**): type I-331 structure when $F = 26\%$; (**f**) type I-331 structure when $F = 49\%$.
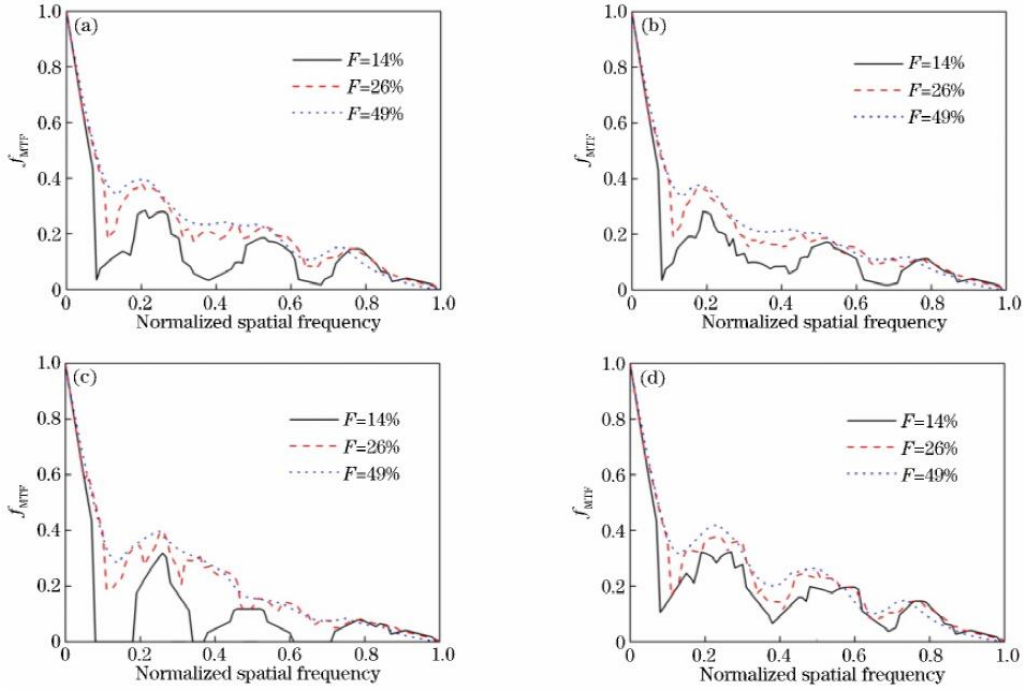
Figure 6. MTF as a function of fill factor F for two different structures. **(a)**: type II-312 structure in horizontal direction; **(b)**: type II-312 structure in vertical direction; **(c)**: type I-331 structure in horizontal direction; **(d)**: type I-331 structure in vertical direction.

modulation transfer function value of II-312 structure is 0 at the normalized frequency of 1.0, while the modulation transfer function value of I-331 structure is reduced to 0 at the normalized frequency of 0.09. That is, when the filling factor is 14%, the II-312 structure has a larger actual cutoff frequency than the I-331 structure in the horizontal direction. When the filling factor is 26%, the modulation transfer function of I-331 structure is 0.02 larger than that of II-312 structure. When the fill factor is 49%, the modulation transfer function value of II-312 structure is larger than that of I-331 structure in the low, middle and high frequency regions. The great value of modulation transfer function of II-312 and I-331 structure is 0.4. In the low frequency region, the modulation transfer function value of II-312 structure is smaller than that of I-331 structure, while in the middle and high frequency region, the modulation transfer function value of II-312 structure is larger than that of I-331 structure. The normalized frequencies in the horizontal direction of the II-312 structure show good characteristics in the middle and high frequencies.

The cutoff frequencies of type II-312 and I-331 structure in vertical direction are shown in **Figure 6b** and **6d**. The modulation transfer function values are larger than those of the II-312 structure. The number of overlapping submodulation transfer functions in the vertical direction is significantly higher for the I-331 structure than for the II-312 structure. When the filling factor is different, the fluctuation of the modulation transfer function curve of the II-312 structure tends to be flat in the mid-frequency region. From the modulation transfer function curves of the two structures in different directions, it can be seen that the increase of the aperture array redundancy can enhance the response of the modulation transfer function in some spatial frequency directions, but it can also reduce the response value at other frequencies and even cause the zero point to appear earlier. In addition, it can be seen from **Figure 5** that the modulation transfer functions of these two structures are not circularly symmetric.

4.4 Other characteristic parameters

Table 2 and **Table 3** show the calculated characteristic indexes for the II-312 and I-331 structures, respectively, where: D_r is the actual equivalent aperture; ρ_r is the actual spatial cutoff frequency; ρ_D is the cutoff frequency of the enclosing aperture; $\alpha_{MTF,mid}$ is the intermediate frequency characteristic characterizing the modulation transfer function[14], which is the average value of the modula-

Table 2. Characteristic indexes of type II-312 structure

F/%	Ratio of practical effective diameters D_r/D	Ratio of average f_{MTF}	ρ_r/ρ_D	$\alpha_{MTF,mid}$
20	0.8902	0.0973	0.7925	0.0465
26	0.8988	0.1080	0.8079	0.0519
33	0.9107	0.1195	0.8294	0.0566
41	0.9586	0.1254	0.9190	0.0598
49	0.9623	0.1232	0.9259	0.0578

Table 3. Characteristic indexes of type I-331 structure

F/%	Ratio of practical effective diameters D_r/D	Ratio of average f_{MTF}	ρ_r/ρ_D	$\alpha_{MTF,mid}$
20	0.7938	0.0834	0.6322	0.0395
26	0.8221	0.0961	0.6758	0.0459
33	0.8683	0.1136	0.7539	0.0537
41	0.9545	0.1258	0.9108	0.0599
49	0.9588	0.1234	0.9194	0.0582

tion transfer function in the range of the subaperture cutoff frequency and the enclosing circular aperture cutoff frequency. From **Table 2** and **Table 3**, it can be seen that for these two structures, D_r/D and ρ_r/ρ_D gradually increase as the filling factor increases. For the same filling factor, the high redundancy of the I-331 structure leads to an increase in the inhomogeneity of its optical transfer function and an increase in the probability of zero frequency. By numerical calculation, the actual cut-off spatial frequency and the actual equivalent aperture value of the II-312 structure are larger than those of the I-331 array structure. The maximum baseline lengths of the two structures are the same, and the maximum cutoff space normalized frequency is 1. When these two structures have the same filling factor, the average modulation transfer function and the modulation transfer function IF characteristics are close to each other. As the filling factor decreases, the actual cutoff frequency of the I-331 structure decreases rapidly after the filling factor exceeds 41%, which reflects the rapid degradation of the modulation transfer function, while the actual cutoff frequency of the II-312 structure shows a gradual decrease. From Section 4.2, it can be known that the redundancy of the I-331 structure is about 6 times higher than that of the II-312 structure. The high redundancy of the I-331 structure is the main reason for the degradation of its modulation transfer function when the filling factor decreases. Therefore, the redundancy of the aperture array should be reduced under the premise of ensuring the imaging quality. When the filling factor reaches the maximum, the values of the average

modulation transfer function and the IF characteristics of the modulation transfer function are not optimal for either the I-331 or the II-312 structure. The comparison of these 2 structures shows that the image quality deteriorates when the d_0 increases beyond a certain threshold. Therefore, to achieve the best imaging quality, it is important to select the appropriate d_0.

The actual equivalent aperture D_r is the diameter of the circular aperture with equal modulation transfer function area within the actual cutoff frequency of the sparse aperture system, calculated as follows:

$$D_r = \left[\frac{4}{\pi} \int_0^{2\pi} \int_0^{\rho_D} \alpha_{MTF,th}(\rho,\theta)\, d\rho d\theta \right]^{\frac{1}{2}}$$

(11)

Where:

$$\alpha_{MTF,th}(\rho,\theta) = \begin{cases} 1, & \alpha_{MTF}(\rho,\theta) > 0, \rho < (\rho_r)_\theta \\ 0, & \alpha_{MTF}(\rho,\theta) = 0 \end{cases}$$

(12)

Where: $\alpha_{MTF,th}$ is the modulation transfer function within the actual cutoff frequency; θ is the angular direction of the sub-modulation transfer function distribution in the spectral plane; $(\rho_r)_\theta$ is the actual spatial cutoff frequency in the direction of θ. The average modulation transfer function is the average value of the modulation transfer function within the enclosing aperture cutoff frequency. Let

$$g(\rho,\theta) = \begin{cases} f_{MTF}(\rho,\theta), & \rho < (\rho_r)_\theta \\ 0, & \rho \geq (\rho_r)_\theta \end{cases}$$

(13)

where: g is the modulation transfer function within the enclosing aperture cutoff frequency.

Then

$$A_{\text{MTF}} = \frac{\int_0^{2\pi} \int_0^{\rho_D} g(\rho, \theta) \rho \mathrm{d}\rho \mathrm{d}\theta}{\pi \rho_d^2}$$

(14)

where: A_{MTF} is the average of the modulation transfer function within the enveloping aperture cutoff frequency; $\alpha_{\text{MTF,mid}}$ is used to characterize the response of the integrated aperture system in the medium and high frequency region, and its expression is

$$\alpha_{\text{MTF,mid}} = \frac{\int_0^{2\pi} \int_{\rho_d}^{\rho_D} g(\rho, \theta) \rho \mathrm{d}\rho \mathrm{d}\theta}{\int_0^{2\pi} \int_{\rho_d}^{\rho_D} \rho \mathrm{d}\rho \mathrm{d}\theta} = \frac{\int_0^{2\pi} \int_{\rho_d}^{\rho_D} g(\rho, \theta) \rho \mathrm{d}\rho \mathrm{d}\theta}{2\pi (\rho_D^2 - \rho_d^2)}$$

(15)

where: ρ_d is the cutoff frequency of the subaperture.

4.5 Comparison of radial multiplet mirror and composite toroidal structure
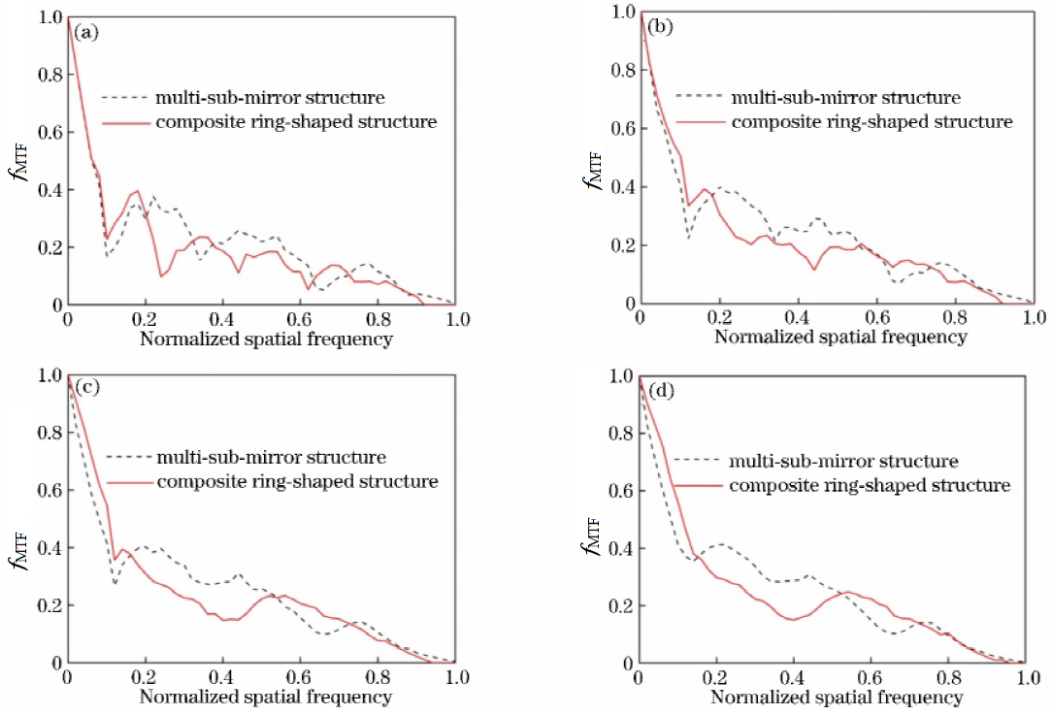
Figure 7. Comparison of MTFs between multi-sub-mirror structure (type II-312) and composite ring-shaped structure with different fill factors (in horizontal direction). **(a)**: $F = 20\%$; **(b)**: $F = 26\%$; **(c)**: $F = 33\%$; **(d)**: $F = 39.6\%$.

Table 4. Characteristic indexes of composite ring-shaped structure with different fill factors

$F/\%$	Ratio of practical effective diameters D_r/D	Ratio of average f_{MTF}	ρ_r/ρ_D	$\alpha_{\text{MTF,mid}}$
20.0	0.7123	0.0798	0.6109	0.0364
26.0	0.7816	0.0912	0.6678	0.0412
33.0	0.8441	0.1091	0.7489	0.0512
39.6	0.8913	0.1201	0.8596	0.0521

The composite array structure is a ture built on a typical optically sparse aperture array. Zhao *et al.*[15] proposed a composite toroidal structure with Golay3 as the basic unit, a composite Goaly6 structure, and a composite three-arm structure. When $N = 24$, only the composite toroidal structure meets the requirement of the number of submirrors, and the rotationally symmetric structure of the subarray in the composite toroidal structure is optimal. In this paper, the radial multi-submirror (type II-312) is selected for comparison with the composite toroidal structure. The maximum filling factor F_{max} of the composite toroidal structure can be calculated. **Figure 7** shows the modulation

transfer function curves along the horizontal direction of the radiating multiplex mirror structure (type II-312) and the composite toroidal structure at different filling factors.

From the calculation, it can be seen that the composite toroidal structure has a larger redundancy than the multi-submirror structure, which leads to a reduced frequency coverage of the composite toroidal structure and a premature zero frequency region between the peaks, so the actual cut-off frequency of the composite toroidal structure is lower. **Table 4** shows the characteristic index of the composite ring structure. Comparing the characteristic indexes in **Table 4** with those in **Table 2**, it can be further precisely concluded that the actual equivalent aperture, actual cutoff frequency, average modulation transfer function, and IF characteristics of the multiple sub-mirror structure (type II-312) are better than those of the composite toroidal structure.

5. Discussion

The radial multiplet mirror array structure is a sparse aperture structure different from the multicircular structure, Golay structure and three-armed structure. In this paper, we analyzed the distribution characteristics of radial multiplet mirrors and divided the multiplet mirror array into 2 types of structures with limited parameters. The profile and top view of the modulation transfer function, two-dimensional modulation transfer function curves and various characteristic indexes of the two different structures are calculated by using MATLAB software, and the structural characteristics and imaging properties of the multiplexed mirror array are compared with those of the composite toroidal structure. The results show that when the average modulation transfer function and the IF characteristics of the modulation transfer function of the two structures are close to each other, the type II structure with larger actual equivalent aperture and actual cutoff frequency and lower redundancy is selected. The type-II structure has some advantages in imaging. The liquid lens-based multiple sub-mirror array structure uses dimensionless approximation parameters, so the conclusion is suitable for arbitrary circumscribed circle size.

Compared with the composite toroidal structure, the actual cutoff frequency and the actual equivalent aperture of the radiative multiplet mirror structure are larger when the filling factor is the same, which is of practical value for the imaging of multiplet mirrors and the optimization of arrays.

Conflict of interest

The authors declare that they have no conflict of interest.

References

1. Meinel AB, Meinel MP. Large sparse-aperture space optical systems. Optical Engineering 2002; 41(8): 1983–1994.
2. Meinel AB. Aperture synthesis using independent telescopes. Applied Optics 1970; 9(11): 2501–2504.
3. Liu L, Jiang YS, Wang HY, *et al*. Novel array configuration and its optimization for sparse aperture imaging systems. Optical Engineering 2011; 50(5): 053202.
4. Yi HW, Li Y, Fan C. Xishu kongjing dengbian liukongjing jiegou yanjiu (Chinese) [Research on pupil configuration of equilateral six sub-apertures sparse aperture system]. Acta Photonica Sinica 2007; 36(11): 2062–2065.
5. Wu Q. Xishu kongjing guangxue xitong chengxiang yanjiu (Chinese) [Study on the sparse aperture optical systems] [PhD thesis]. Suzhou: Suzhou University; 2006.
6. Wu Q, Qian L, Shen W. Fuhe sanzijing xishu kongjing guangtong jiegou de yanjiu (Chinese) [Research on pupil configuration of dual three sub-apertures sparse aperture system]. Acta Optica Sinica 2006; 26(2): 187–192.
7. Harvey JE, Rockwell RA. Performance characteristics of phased array and thinned aperture optical telescopes. Optical Engineering 1988; 27(9): 762–768.
8. Han J, Wang D, Liu H, *et al*. Guangxue xishu kongjing chengxiang fuhe kongjing zhenlie jiegou yanjiu (Chinese) [Multiple-array configuration design of optical sparse-aperture imaging system]. Journal of Optoelectronics Laser 2007; 18(6): 649–652.
9. Fiete RD, Tantalo TA, Calus JR, *et al*. Image quality of sparse-aperture designs for remote sensing. Optical Engineering 2002; 41(8): 1957–1969.
10. Xie N, Zhang N, Zhao R, *et al*. Jiaoliu zuoyong xia dianrunshi yeti toujing dongtai guocheng de ceshi yu fenxi (Chinese) [Test and analysis of the dynamic procedure for electrowetting-based liquid lens under alternating current voltage]. Acta Physica Sinica 2016; 65(22): 224202.
11. Zhao R, Hua X,Tian Z, *et al*. Dianrunshi shuangyeti bianjiao toujing (Chinese) [Electrowettingbased variable-focus double-liquid lens].

Optics and Precision Engineering 2014; 22(10): 2592–2597.

12. Zhou C, Wang Z, Zhang S, *et al*. Dakongjing yanshe shouxian guangxue hecheng kongjing xitong MTF zhong de buchang (Chinese) [Large aperture diffraction limited optical synthetic aperture system intermediate frequency MTF compensation]. Acta Optica Sinica 2018; 38(4): 169–175.

13. Liu L, Jiang Y. Principle and application of synthetic aperture imaging. Beijing: National Defense Industry Press; 2013. p. 45–78.

14. Miller N, Duncan B, Dierking M. Resolution enhanced sparse aperture imaging. 2006 IEEE Aerospace Conference; 2006 Mar 4–11; Big Sky, MT, USA. New York: IEEE; 2006. p. 1655904.

15. Zhao J, Wang D, Zhang Y, *et al*. Guangxue xishu kongjing xitong fuhe zhenlie gouzao dui xitong chengxiang de yingxiang (Chinese) [Effect of different designs of the multiple-array configuration on imaging of optical sparse aperture systems]. Chinese Journal of Lasers 2009; 36(4): 934–939.

49